

# Opportunistic hip fracture risk prediction in Men from X-ray: Findings from the Osteoporosis in Men (MrOS) Study

Lars Schmarje<sup>1,\*</sup>, Stefan Reinhold<sup>1</sup>, Timo Damm<sup>2</sup>, Eric Orwoll<sup>3</sup>, Claus-C. Glüer<sup>2</sup>, and Reinhard Koch<sup>1</sup>

<sup>1</sup> MIP, Computer Science, Kiel University {las,sre,rk}@informatik.uni-kiel.de

<sup>2</sup> MOINCC, Kiel University, Germany {timo.damm,glueer}@rad.uni-kiel.de

<sup>3</sup> Oregon Health & Science University, United States orwoll@ohsu.edu

\* Corresponding author: las@informatik.uni-kiel.de

**Abstract.** Osteoporosis is a common disease that increases fracture risk. Hip fractures, especially in elderly people, lead to increased morbidity, decreased quality of life and increased mortality. Being a silent disease before fracture, osteoporosis often remains undiagnosed and untreated. Areal bone mineral density (aBMD) assessed by dual-energy X-ray absorptiometry (DXA) is the gold-standard method for osteoporosis diagnosis and hence also for future fracture prediction (prognostic). However, the required special equipment is not broadly available everywhere, in particular not to patients in developing countries. We propose a deep learning classification model (FORM) that can directly predict hip fracture risk from either plain radiographs (X-ray) or 2D projection images of computed tomography (CT) data. Our method is fully automated and therefore well suited for opportunistic screening settings, identifying high risk patients in a broader population without additional screening. FORM was trained and evaluated on X-rays and CT projections from the Osteoporosis in Men (MrOS) study. 3108 X-rays (89 incident hip fractures) or 2150 CTs (80 incident hip fractures) with a 80/20 split (training / validation) were used. We show that FORM can correctly predict the 10-year hip fracture risk with a validation AUC of  $81.44\% \pm 3.11\%$  /  $81.04\% \pm 5.54\%$  (mean  $\pm$  STD) including additional information like age, BMI, fall history and health background across a 5-fold cross validation on the X-ray and CT cohort, respectively. Our approach significantly ( $p < 0.01$ ) outperforms previous methods like Cox Proportional-Hazards Model and FRAX<sup>®</sup> with  $70.19 \pm 6.58$  and  $74.72 \pm 7.21$  respectively on the X-ray cohort. Our model outperform on both cohorts hip aBMD based predictions (validation AUC  $82.67\% \pm 0.21\%$  vs.  $71.82\% \pm 0.50\%$  and  $78.41\% \pm 0.33$  vs.  $76.55\% \pm 0.89\%$ ). We are confident that FORM can contribute on improving osteoporosis diagnosis at an early stage.

**Keywords:** fracture risk prediction · osteoporosis · opportunistic screening

## 1 Introduction

Osteoporosis is a wide-spread systemic disease that leads to deterioration of bone mass and micro structure and subsequently to decreased bone strength inducing an increased fracture risk [21]. According to the United States Preventive Services Task Force, the lifetime risk of an osteoporotic fracture is about 50% in women and about 20% - 25% in men [32,20]. While osteoporosis affects all bones, fractures of the spine and hip are the most frequent. Especially hip fractures lead to increased morbidity, decreased quality of life and increased mortality — 20% of osteoporotic hip fractures lead to death within six month[6]. Being a silent disease before fracture, osteoporosis often remains undiagnosed and consequently untreated. Especially in men, only about 2% are diagnosed before fracture [20].

The gold-standard method for osteoporosis diagnosis is based on areal bone mineral density (aBMD) assessed by dual-energy X-ray absorptiometry (DXA). This modality is in general broadly available to patients in many countries worldwide - with some degree of uneven distribution among industrial nations. In developing countries in African and South America and the Middle East, the availability is poor [15,9]. More elaborate methods like volumetric bone mineral density (vBMD) assessed by quantitative computed tomography (QCT) or finite element modeling (FEM) of bone strength, either based on QCT or DXA, have shown to be superior to standard aBMD [37,18,27,33,1]. However, all these method either require special equipment, protocols or domain experts and the prognosis of osteoporotic fractures is an even more challenging and labor-intensive task.

In this paper, we focus on fracture prognosis in an opportunistic screening scenario: whenever radiographic imaging is available an automated method inspects the image for indicators of possible future fractures. Patients with high fracture risk could be advised to see a specialist to confirm the risk and possibly initiate preventive actions. Due to their outstanding capacity to learn task-relevant image features such methods - in particular convolutional neural networks (CNN) – have outperformed “classical” machine learning algorithms in many image analysis tasks[29,23,22,25,8,24]. We predict the risk of future fractures (prognostics), in contrast to detecting acute osteoporosis or incident fractures (diagnostics).

The goal is to develop a pipeline that can be used for opportunistic screening and hence beneficially leverage additional risk factors. For this purpose we propose a two-stage deep learning based classification method that is able to predict the 10-year fracture risk using only X-ray or CT scans and optionally case history as inputs. We train and evaluate our method on a dataset from the Osteoporotic Fractures in Men (MrOS<sup>4</sup>) study. We restrict our main evaluation to information (e.g. age, weight, height, etc.) that would be collectible in this setting; other information (e.g. aBMD) is only included for comparison.

**Our key contributions are:** (1) a fully automated system that can be used in an prognostic opportunistic screening scenario, (2) val AUC results of 81.44% and 81.04% on the X-ray and CT cohort respectively. (3) we signifi-

<sup>4</sup> The Osteoporotic Fractures in Men (MrOS) Study: <https://mrosonline.ucsf.edu>

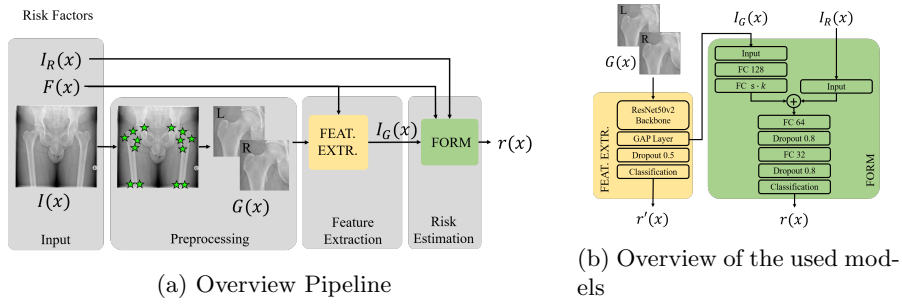


Fig. 1: Illustration<sup>5</sup> of proposed pipeline. (a) Inputs and pipeline stages: preprocessing, feature extraction and risk estimation. (b) Detailed view of models in (a) (yellow, green). Parameter of fully connected (FC) layers: number of hidden neurons. Further information can be found in section 2.

cantly outperform previous methods like Cox Proportional-Hazards Model and FRAX<sup>®</sup> in the opportunistic use case and achieve improved or competitive results for non-opportunistic settings, (4) beneficial integration of clinical risk factors with image based features into a deep learning pipeline.

### 1.1 Related Work

In the past numerous risk factors for osteoporotic fractures were identified. Among them are increased age, low body mass index (BMI), previous fragility fractures, smoking or alcohol intake. While aBMD alone has shown to be a not sufficiently sensitive predictor for screening applications[16], the combination with other risk factors (RF) is more promising. In [26] Schousboe et al. found that additional RF are better than a model using only aBMD and age for vertebrae fracture prediction. Elaborate statistical shape and density modeling based on volumetric QCT data has proven to be superior to DXA based aBMD models[2] for hip fracture prognosis. Hippisley-Cox et al. proposed the QFractureScores algorithm [11] to predict the 10-year fracture risk. FRAX<sup>®</sup> [16] is a fracture risk assessment tool that uses various RF with or without additional aBMD measurements to predict a 10-year fracture risk. The National Osteoporosis Foundation included FRAX<sup>®</sup> in its guidelines to recommend aBMD measurements or even treatment based on predicted fracture risk[34]. Su et al. [30] used classification and regression trees (CART) on common RF to predict fracture risk on the MrOS data and found a slight improvement over FRAX<sup>®</sup> based predictions. Treece et al. [31] used cortical bone mapping (CBM) to predict osteoporotic fractures in the MrOS study. They found that adding CBM to aBMD can improve fracture prognosis performance. Most of these methods do, however,

<sup>5</sup> Example image and key points only for illustrative purpose; image source <https://radiopaedia.org/cases/normal-hip-x-rays>

require special protocols, modalities or in-depth interviews of the patient that might not be applicable to an opportunistic screening setting.

In [19], Pickhardt et al. were able to discriminate manually between patients with osteoporosis and with normal BMD using opportunistic abdomen CTs. Recently, several related deep learning based approaches for semi-automated osteoporosis diagnosis have been presented. Ho et al. [12] and Hsieh et al. [13] used a deep learning architecture to predict DXA based aBMD from hip X-ray. Other works like [14] or [36] detect osteoporosis directly from image features of X-ray using end-to-end classification networks. They achieve high classification performance ( $AUC > 0.9$ ) which could even be slightly improved [36] by incorporating clinical risk factors ( $AUC > 0.92$ ). However, this diagnosis task is not comparable to the prognosis task that we target in our work. For prognosis, Hsieh et al. [13] used their predicted aBMD as input to FRAX<sup>®</sup> to predict a 10-year fracture risk. However, since the performance of this combination is limited by the performance of DXA-based aBMD, they were unable to achieve any improvement over baseline FRAX<sup>®</sup> + (DXA-based) aBMD.

Recently, Damm et al. proposed a fully automatic deep learning method to predict hip fractures in women using X-rays from the Study of Osteoporotic Fractures (SOF<sup>6</sup>)[5]. They showed that deep learning based methods are able to improve the prognostic performance of classical aBMD based models while maintaining a high degree of automation. However, they did not investigate additional risk factors and other image modalities as input such as CT.

## 2 Method

We propose an automatic image processing pipeline for the prediction of **F**uture **O**steoporotic **F**ractures **R**isk in **M**en for **H**ips (FORM). The pipeline consists of a preprocessing, a feature extraction and a risk estimation stage for each patient  $x$ . An overview is given in Figure 1a.

### 2.1 Preprocessing

The proposed method should be able to process 2D X-rays as well as 3D CT scans. To share both architecture and hyperparameters for both input modalities, we compute 2D projections from the 3D CT scans. This way, however, most of the 3D structural information from the CT scans is lost. To fully exploit the 3D information, a native 3D CNN could have been used, but this would have resulted in a much larger memory footprint and thus higher hardware requirements. Therefore, in this work, we have focused at first on confirming the usefulness of CT image data for predicting future fractures. In the following, the CT projections will be referred to simply as CT.

A Hough transform is used to detect the QCT calibration phantom that is present in all scans in order to remove it and the underlying table from the

<sup>6</sup> The Study of Osteoporotic Fractures (SOF:) <https://sofonline.ucsf.edu>

image<sup>7</sup>. Since the phantom is always located beneath the patient, the scans can easily be cropped to exclude the phantom and the table. The cropped 3D scans are then projected onto the coronal plane and re-scaled by a constant value to achieve pixel value range of  $[0, 1]$ . We also investigated a re-scaling per patient to investigate the influence of the scanner HU calibration; results on these normalized CTs (CTN) are reported in the supplement.

CT projections and X-ray images  $I(x)$  were split into two halves depicting the right and the left hip, respectively; images of the left hip were vertically flipped. A key point detection CNN inspired by [5] were used to detect 12 key points located around the femur. The key point detector was trained jointly on 1797 X-ray images and 208 CT projections (104 CT, 104 CTN) with manually annotated key point positions. The key point CNN classifies the image halves into three classes: *complete* (full proximal femur is visible), *incomplete* (proximal femur not completely visible) and *implant*. A selection of key points is used to crop the image to the proximal femur region (including the trochanter minor and the femoral head). These cropped images  $G(x)$  are included in the dataset if the predicted class is *complete* with a confidence above 0.01 (X-ray) or 0.2 (CT).

The risk factors (RF) are additional information about the patient which might improve the hip fracture risk prediction. As we are not interested on the impact of a single risk factor, but rather whether the information is helpful in combination with image data, we grouped the RF for better referencing: *Base*, *Multiple*, *aBMD*, *FRAX*<sup>®</sup> and *TBS*[28]. The details are summarized in the supplementary. The *Base* group contains basic patient information like age and BMI. The *Multiple* group extends *base* and adds additional information from the case history and health background. This information might not be present in clinical routine but could be acquired from every patient via a questionnaire (non-densitometric). The other groups consists of other well-known risk factors, also including densitometry. For densitometry, additional imaging and evaluation is required and thus is not suitable for opportunistic screening. We included these risk factors as a comparison. 52 patients were excluded from the dataset due to missing data for at least one risk factor.

## 2.2 Feature Extraction

We train a CNN as a Feature Extractor with output  $r'(x)$  on the cropped femur images  $G(x)$  and extract the predicted Global Average Pooling (GAP) Features of the network. These GAP features  $I_G(x) \in \mathbb{R}^{2048}$  are used as input for the next pipeline stage. For the training of the CNN, a ground truth label  $F_t(x)$  is needed indicating whether the patient  $x$  will fracture by time horizon  $t$  (e.g. 10 years) or not. All patients with unknown fracture status, e.g., due to death before time horizon  $t$ , were excluded from the dataset. This renders all predicted risks conditional on the patient survival to time horizon  $t$ . This is acceptable for

<sup>7</sup> In the MrOS study, the phantoms are used to calibrate HU to BMD. In this work no BMD calibration is performed for a more realistic opportunistic screening setting

an opportunistic screening because we need to screen all patients regardless of whether or not they would survive to  $t[3]$  but might introduce a bias.

FORM has a ResNet50v2 [10] backbone pretrained on ImageNet[17] with three additional layers depicted in Figure 1b. Data was augmented with random flips, zooms and color changes; classes were weighted. Input image dimensions were 96x96 (CT) or 224x244 (X-ray) pixels. Training was performed for 50 epochs, a batch size of 36, learning rate of  $10^{-4}$ , dropout (0.5)<sup>8</sup>. A cross-entropy loss was used and input samples were weighted based on their class distribution. GAP features  $G(x)$  were extracted after early stopping (see subsection 3.1 for details about the metrics).

### 2.3 Risk Estimation

For the risk estimation  $r(x)$ , we train a multi layer perceptron (MLP) to predict hip fractures up to the horizon  $t$  with the target  $F_t(x)$ . Its input can be varied: GAP-Features  $I_G(x)$ , RF  $I_R(x)$  or both. Categorical data is one hot encoded and concatenated with normalized continuous data into the input vector  $I_R(x)$ . Using many RF together with the high-dimensional GAP features might make the model more prone to overfitting because individual datapoints become more distinct. This is counteracted by a high dropout rate. To prevent imbalancing between  $I_G(x)$  and  $I_R(x)$  due to high dimensional differences (e.g. 2048 vs. 4) an MLP with 128 and  $s \cdot k$  hidden nodes is used to reduce the dimension of the GAP features before concatenation. Here  $k$  is the dimension of  $I_R(x)$  and  $s$  is a scaling hyperparameter set to 5. Hyperparameters are mostly shared in Feature Extraction and Risk Estimation and the differences are illustrated in Figure 1b. An ablation study to inspect the impact of the hyperparameters is included in the supplementary material and discussed in subsection 3.3.

## 3 Evaluation

### 3.1 Datasets and Baseline Methods

For training and evaluation, we used the dataset from the Osteoporosis in Men (MrOS) study. Patients were followed for more than 10 years. We used the first hip fracture that occurred after the baseline visit as our primary outcome. A detailed overview of the datasets statistics for the X-ray and the CT cohort in comparison to the complete study population can be found in Table 1. The number of included patients  $n$  is decreased by about one third of the overall number of patients with available image data due to censoring and excluded image halves (e.g. due to implants). During a 5 / 10 year follow-up 1.45% and 3% of the men suffered a hip fracture, respectively. This low number of cases limits the generalizability but it is possible to identify trends which repeat across different

<sup>8</sup> Implemented in Tensorflow 2.4, source code will be release on publication, experiments executed on Nvidia RTX 3090, inference < 1 second per image

<sup>8</sup> <https://mrosonline.ucsf.edu>, Update august 2021

Table 1: Statistics for three different cohorts (all, CT or X-Ray data available). For each cohort we give the statistics for the complete cohort and with respect to the hip fracture horizon with (w) and without (w/o) fracture (fx).  $n$  represents the number of samples. Age is given as relative percentage for a specific range from  $n$ . Training / Validation refer to the number of used images in the respective sets in the first fold. - means that no data was used for training or validation. All other risk factors are given as mean (STD in brackets).

	Cohort All			Cohort CT					Cohort X-Ray			
	$t = 10$ year			$t = 10$ year			$t = 5$ year		$t = 10$ year			
	all	w/o fx	w fx	all	w/o fx	w fx	w/o fx	w fx	all	w/o fx	w fx	
$n$	5994	4004	185	3165	2150	80	2198	32	3895	3108	89	
Age [%]	64-69	29.51	36.69	10.27	30.74	37.86	16.25	37.44	12.50	32.99	37.32	15.73
	70-74	28.50	31.87	16.22	28.44	32.00	15.00	31.71	9.38	30.40	31.66	19.10
	75-79	24.11	21.98	33.51	23.70	21.44	37.50	21.84	34.38	23.90	22.30	39.33
	80+	17.88	9.47	40.00	17.12	8.70	31.25	9.01	43.75	12.71	8.72	25.84
Height [m]	1.74	1.75	1.73	1.74	1.75	1.74	1.75	1.72	1.74	1.74	1.74	
	(0.07)	(0.07)	(0.06)	(0.07)	(0.07)	(0.06)	(0.07)	(0.06)	(0.07)	(0.07)	(0.06)	
BMI [ $\frac{kg}{m^2}$ ]	25.90	26.00	25.11	25.80	25.89	24.77	25.86	24.68	25.86	25.90	24.86	
	(3.65)	(3.54)	(3.63)	(3.60)	(3.48)	(3.38)	(3.49)	(3.02)	(3.57)	(3.48)	(3.65)	
Femoral aBMD [ $\frac{g}{cm^2}$ ]	0.78	0.79	0.66	0.78	0.79	0.65	0.79	0.62	0.79	0.79	0.68	
	(0.13)	(0.13)	(0.11)	(0.13)	(0.13)	(0.08)	(0.13)	(0.08)	(0.13)	(0.12)	(0.10)	
Spine aBMD [ $\frac{g}{cm^2}$ ]	1.07	1.07	1.01	1.07	1.06	1.00	1.06	0.98	1.07	1.07	1.00	
	(0.19)	(0.18)	(0.19)	(0.19)	(0.18)	(0.16)	(0.18)	(0.19)	(0.18)	(0.18)	(0.20)	
Avg. TBS	1.23	1.23	1.19	1.23	1.24	1.20	1.24	1.17	1.24	1.24	1.19	
	(0.13)	(0.13)	(0.13)	(0.13)	(0.12)	(0.12)	(0.12)	(0.13)	(0.12)	(0.12)	(0.12)	
FRAX <sup>®</sup> [%]	4.14	3.14	7.04	4.01	3.04	6.29	3.07	8.53	3.54	3.07	5.76	
	(4.39)	(3.07)	(5.67)	(4.28)	(2.93)	(5.85)	(2.94)	(7.97)	(3.56)	(2.89)	(4.87)	
FRAX <sup>®</sup> (w. aBMD) [%]	4.45	3.38	10.86	4.33	3.35	10.47	3.45	14.38	3.85	3.34	9.41	
	(5.54)	(4.04)	(9.09)	(5.41)	(3.95)	(8.92)	(4.12)	(9.41)	(4.74)	(3.95)	(8.56)	
Training	-	-	-	-	3403	128	3478	53	-	4353	107	
Validation	-	-	-	-	790	27	810	7	-	1086	35	

modalities, horizons and settings. Therefore, we use the same training validation split based on the patient IDs across all experiments for the respective cohorts. We used area under the receiver-operator curve (AUC) as the main metric. A 5-fold cross-validation was used to ascertain the validity of the comparison with the established baselines; across folds validation means and standard deviations (STD) are reported. To ensure reproducibility training was repeated 10 times for deep learning models. In the ablation studies, we analyzed only one fold across 10 repetitions and report means with their standard errors (SE). A two-sided Welch-Test[35] was used to compare the calculated means.

The folds are fixed for all input combinations. However, since not all patients have both, X-ray and CT data different subgroups of the training and validation data were used for each modality. This means that the different cohorts are similar but can not be directly compared. Therefore, we compare across both cohorts with different inputs / models (e.g. FRAX<sup>®</sup>). Matching the X-ray and CT cohorts would have resulted in too few fracture cases. Sampling was performed on a per-patient basis, ensuring the two image halves for one patient always are in the same fold.

As baselines a Cox Proportional-Hazards Model (Cox) [4] and FRAX<sup>®</sup> was used. For the Cox model the same input as to our model FORM was used.

Table 2: Cross-validation results (mean val. AUC  $\pm$  STD) – columns: different methods / inputs; rows: cohort. Bold: results within a one percent margin of the best for each cohort.

Cohort	FORM			Cox			FRAX <sup>®</sup>
	GAP	GAP + Base	GAP + Multiple	GAP	GAP + Base	GAP + Multiple	
X-Ray	<b>81.57 <math>\pm</math> 3.13</b>	<b>81.09 <math>\pm</math> 3.18</b>	<b>81.44 <math>\pm</math> 3.11</b>	61.14 $\pm$ 16.80	70.26 $\pm$ 5.71	70.19 $\pm$ 6.58	74.72 $\pm$ 7.21
CT	77.53 $\pm$ 5.81	<b>80.66 <math>\pm</math> 3.75</b>	<b>81.04 <math>\pm</math> 5.54</b>	67.56 $\pm$ 23.97	73.69 $\pm$ 9.22	75.35 $\pm$ 9.11	74.74 $\pm$ 5.70

Table 3: Comparison fracture risk prediction – columns: different inputs which were used to train FORM; rows: different cohorts. All scores are given as mean val AUC  $\pm$  SE. Significant differences between the first and the other columns are marked italic ( $p < 0.05$ ) or bold ( $p < 0.01$ ). † input not used for FORM

Cohort	GAP + Multiple	Base	Multiple	GAP	GAP + Base	FRAX <sup>®</sup> †
X-Ray	78.41 $\pm$ 0.33	<b>66.38 <math>\pm</math> 1.76</b>	<b>69.67 <math>\pm</math> 0.99</b>	<i>77.24 <math>\pm</math> 0.30</i>	77.81 $\pm$ 0.38	77.43
CT	82.67 $\pm$ 0.21	<b>60.89 <math>\pm</math> 0.73</b>	<b>67.03 <math>\pm</math> 0.93</b>	82.58 $\pm$ 0.21	82.48 $\pm$ 0.24	75.94

(a) Non-densitometric Settings

Cohort	GAP + Multiple	aBMD + Base	FRAX <sup>®</sup> + aBMD + Base	TBS + Base	FRAX <sup>®</sup> + aBMD†
X-Ray	78.41 $\pm$ 0.33	<b>76.55 <math>\pm</math> 0.89</b>	<b>81.50 <math>\pm</math> 0.83</b>	<b>72.66 <math>\pm</math> 1.34</b>	80.92
CT	82.67 $\pm$ 0.21	<b>71.82 <math>\pm</math> 0.50</b>	<b>81.08 <math>\pm</math> 0.34</b>	<b>71.56 <math>\pm</math> 0.39</b>	79.19

(b) Densitometric Settings

However, the low variance of the high dimensional GAP features lead to a numerical degeneration of the Cox model. This was circumvented by performing a dimensionality reduction using Principal Component Analysis (PCA) [7] of the GAP feature space. The Cox model was fitted on the training data and used for prediction on the validation data. Best performing number of PCA components are reported based on the validation set.

### 3.2 Results

The proposed method (FORM), a Cox Proportional-Hazards Model (Cox) and FRAX<sup>®</sup> are compared using a five-fold cross-validation analysis in Table 2. It can be seen, that the proposed method outperforms Cox and FRAX<sup>®</sup> on both cohorts by around 6%. In general, using more risk factors in the GAP feature input improves the prediction; this benefit is slightly higher on the CT cohort. Especially for Cox, a high variance without risk factors can be observed which can be credited to one or two folds with significant lower performance (e.g. around 35% on one fold for the X-ray Cohort). The number of the PCA components were 2 and 1 for the X-ray and CT cohort, respectively. While more components lead to improved training scores the values on the validation data degenerate and thus indicate an overfitting. We checked for the Cox models the variables with a significant impact on the prediction on at least two folds. The variables for the



X-ray cohort were age, gap features, smoking, fall history and BMI. For the CT cohort the variables were age, gap features, BMI, cancer and hypertension.

On one fold the power to predict hip fractures were analyzed further by adding comparisons without GAP features and evaluations including densitometric inputs variables in Table 3. Across both cohorts, a significant improvement of around 20% to only using the risk factors group Base or Multiple can be seen. Moreover, a significant improvement of up to one percent is achieved when adding information about risk factors on X-ray and the vanilla FRAX<sup>®</sup> is worse for both cohorts. Overall the image-based result are all similar and within a range of around three percent of 80%. For the densitometric settings, only the usage of Base risk factors is reported, because further information did not improve the results. In the comparison of the best non-densitometric model, with densitometric settings FORM still outperform most risk factors or the vanilla FRAX<sup>®</sup> +aBMD predictor. Only X-ray based imaging is up to three percent worse than FRAX<sup>®</sup> based predictions. We see an improvement of using the FRAX<sup>®</sup> +Base as input to FORM in comparison to the vanilla FRAX<sup>®</sup> predictor.

The ablation study on the CTN for the 10 and 5 year horizon in the supplement shows that changes to the used hyperparameters lead to significant degenerations of up to three percent. Without input merging the additional risk factors can not be beneficially used or even degenerate the results due to overfitting. A lower dropout rate or a larger model which result in faster overfitting have a similar effect. On the CTN data in general more risk factors improve the results by up to one percent.

### 3.3 Discussion

We conclude three major results: (1) FORM outperforms Cox and FRAX<sup>®</sup> on two image cohorts and performs similarly or better even if we include densitometric inputs as comparison, (2) only image information can be used for fracture risk prediction but additional risk factors can help the risk estimation and (3) FORM can leverage the combined information of image information and risk factors better than Cox.

Across all experiments FORM outperforms the other non-densitometric models. Only the densitometric FRAX<sup>®</sup> predictor (including aBMD) performs better on the X-ray cohort than FORM. However, our models do not require additional imaging with DXA. Future research could highlight important image regions for the risk estimation or the importance of additional risk factors which could improve the interpretability and therefore the acceptance of the system in clinical routine.

For Cox and FORM in Table 2, it can be seen that a fracture risk estimation only based on image information is possible and even outperforms predictions only based on risk factors in Table 3. Using additional risk factors as input can improve the results significantly by up to four percent. This shows that risk factors are a valid source for additional information but also that a majority of the information is already encoded in a patient's X-ray or CT.

The Cox model performs in the best case similar or worse than FRAX<sup>®</sup> but is outperformed by FORM. While FRAX<sup>®</sup> might use other input variables, the Cox model is trained with the same inputs as FORM. We conclude that our model can learn from the high dimensional data better than Cox due to two reasons: first, the Cox model required preprocessed inputs via PCA to prevent degeneration. Second, the overfitting prevents adding more than one or two PCA components as input.

In Chapter 2.2, we explained that patients were excluded due to early death. The censored patients cannot be directly evaluated, but their subgroup which survived for at least the first 5 years without a fracture. The number of false positive predicted patients across 20 repetitions are  $3.63\% \pm 0.51\%$  SE and  $5.01\% \pm 0.80\%$  SE for the validation and censored subset, respectively. We conclude that our model is performing at least plausible on this subset.

### 3.4 Limitations and Future Work

This study is based solely on the MrOS dataset, which consists only of men and contains an expected low number of incident (future) fractures. Both issues limit the generalizability of our work but can be verified on other datasets in the future. The identified trends are supported across different cohorts and settings but have to be confirmed on other studies especially including women and with a higher number of fractured cases. 2D projections were used to share architectures between X-ray and CT, but native 3D architectures should be investigated. This study can only analyze the benefits of image data for opportunistic screening in a proof-of-concept fashion, since the strict imaging protocols were imposed for the study. A long term study in clinical routine is required to evaluate the practicability and the evaluation of questions like how many false positive / negatives are acceptable in clinical routine or how the output probability should be calibrated in regard to the sensitivity / specificity trade-off. This will be future work.

## 4 Conclusion

We have shown that X-ray and CT data can be automatically analyzed and processed by our method FORM for opportunistic hip fracture prognosis. We achieved a mean validation AUC of greater than 80% for 10-year hip fracture risk in a five-fold cross-validation in both cohorts based on radiographic and CT data. This is significantly better than previous methods like Cox or FRAX<sup>®</sup> on the same or comparable input. Even in most cases, with additional densitometric RF, our method is significantly better. Overall, we are confident that our method FORM and image input in general are promising candidates for improving the identification of men at high risk of future osteoporotic hip fractures.

## References

1. Black, D.M., Bouxsein, M.L., Marshall, L.M., Cummings, S.R., Lang, T.F., Cauley, J.A., Ensrud, K.E., Nielson, C.M., Orwoll, E.S.: Proximal femoral structure and the prediction of hip fracture in men: a large prospective study using QCT. *Journal of Bone and Mineral Research* **23**(8), 1326–1333 (2008)
2. Bredbenner, T.L., Mason, R.L., Havill, L.M., Orwoll, E.S., Nicoletta, D.P., in Men (MrOS) Study, O.F.: Fracture risk predictions based on statistical shape and density modeling of the proximal femur. *Journal of bone and mineral research* **29**(9), 2090–2100 (2014)
3. Camacho, P.M., Petak, S.M., Binkley, N., Diab, D.L., Eldeiry, L.S., Farooki, A., Harris, S.T., Hurley, D.L., Kelly, J., Lewiecki, E.M., Pessah-Pollack, R., McClung, M., Wimalawansa, S.J., Watts, N.B.: American Association of Clinical Endocrinologists/American College of Endocrinology Clinical Practice Guidelines for the Diagnosis and Treatment of Postmenopausal Osteoporosis—2020 Update. *Endocrine Practice* **26**, 1–46 (2020)
4. Cox, D.R.: Regression Models and Life-Tables. *Journal of the Royal Statistical Society. Series B (Methodological)* (2), 187–220
5. Damm, T., Schmarje, L., Koser, N., Reinhold, S., Yilmaz, E., Krekieleh, N., Lui, L.Y., Cummings, S.R., Koch, R., Glueer, C.C.: Artificial intelligence-driven hip fracture prediction based on pelvic radiographs exceeds performance of DXA: the “Study of Osteoporotic Fractures” (SOF). *Journal of Bone and Mineral Research* **37**, 193–193 (2021)
6. Ebeling, P.R.: Osteoporosis in men: Why change needs to happen. *World Osteoporosis Day Thematic Report International Osteoporosis Foundation*, Nyon (2014)
7. F.R.S., K.P.: LIII. On lines and planes of closest fit to systems of points in space. *The London, Edinburgh, and Dublin Philosophical Magazine and Journal of Science* **2**(11), 559–572 (1901)
8. Grossmann, V., Schmarje, L., Koch, R.: Beyond Hard Labels: Investigating data label distributions. *arXiv preprint arXiv:2207.06224* (jul 2022), <http://arxiv.org/abs/2207.06224>
9. Hamidi, Z.: What’s BMD and What We Do in a BMD Centre? pp. 225–246 (2012). <https://doi.org/10.5772/38953>
10. He, K., Zhang, X., Ren, S., Sun, J.: Deep Residual Learning for Image Recognition. *IEEE Conference on Computer Vision and Pattern Recognition (CVPR)* pp. 770–778 (2015), <http://arxiv.org/abs/1512.03385>
11. Hippisley-Cox, J., Coupland, C.: Predicting risk of osteoporotic fracture in men and women in England and Wales: prospective derivation and validation of QFractureScores. *Bmj* **339** (2009)
12. Ho, C.S., Chen, Y.P., Fan, T.Y., Kuo, C.F., Yen, T.Y., Liu, Y.C., Pei, Y.C.: Application of deep learning neural network in predicting bone mineral density from plain X-ray radiography. *Archives of Osteoporosis* **16**(1), 1–12 (2021)
13. Hsieh, C.I., Zheng, K., Lin, C., Mei, L., Lu, L., Li, W., Chen, F.P., Wang, Y., Zhou, X., Wang, F., Others: Automated bone mineral density prediction and fracture risk assessment using plain radiographs via deep learning. *Nature communications* **12**(1), 1–9 (2021)
14. Jang, R., Choi, J.H., Kim, N., Chang, J.S., Yoon, P.W., Kim, C.H.: Prediction of osteoporosis from simple hip radiography using deep learning algorithm. *Scientific reports* **11**(1), 1–9 (2021)

15. Johnell, O., Kanis, J.A.: An estimate of the worldwide prevalence and disability associated with osteoporotic fractures. *Osteoporosis international* **17**(12), 1726–1733 (2006)
16. Kanis, J.A., Johnell, O., Odén, A., Johansson, H., McCloskey, E.: FRAX™ and the assessment of fracture probability in men and women from the UK. *Osteoporosis international* **19**(4), 385–397 (2008)
17. Krizhevsky, A., Sutskever, I., Hinton, G.E.: Imagenet classification with deep convolutional neural networks. In: *Advances in neural information processing systems*. vol. 60, pp. 1097–1105. Association for Computing Machinery (2012). <https://doi.org/10.1145/3065386>
18. Langsetmo, L., Peters, K.W., Burghardt, A.J., Ensrud, K.E., Fink, H.A., Cawthon, P.M., Cauley, J.A., Schousboe, J.T., Barrett-Connor, E., Orwoll, E.S., Others: Volumetric bone mineral density and failure load of distal limbs predict incident clinical fracture independent of FRAX and clinical risk factors among older men. *Journal of Bone and Mineral Research* **33**(7), 1302–1311 (2018)
19. Pickhardt, P.J., Pooler, B.D., Lauder, T., del Rio, A.M., Bruce, R.J., Binkley, N.: Opportunistic screening for osteoporosis using abdominal computed tomography scans obtained for other indications. *Annals of internal medicine* **158**(8), 588–595 (2013)
20. Prasad, D., Nguyen, M.H.: Chronic hepatitis, osteoporosis, and men: under-recognised and underdiagnosed. *The Lancet Diabetes & Endocrinology* **9**(3), 141 (2021)
21. Salari, N., Ghasemi, H., Mohammadi, L., Rabieenia, E., Shohaimi, S., Mohammadi, M., Others: The global prevalence of osteoporosis in the world: a comprehensive systematic review and meta-analysis. *Journal of orthopaedic surgery and research* **16**(1), 1–20 (2021)
22. Santarossa, M., Kilic, A., von der Burchard, C., Schmarje, L., Zelenka, C., Reinhold, S., Koch, R., Roider, J.: MedRegNet: unsupervised multimodal retinal-image registration with GANs and ranking loss. In: *Medical Imaging 2022: Image Processing*. vol. 12032, pp. 321–333. SPIE (2022)
23. Schmarje, L., Brünger, J., Santarossa, M., Schröder, S.M., Kiko, R., Koch, R.: Fuzzy Overclustering: Semi-Supervised Classification of Fuzzy Labels with Overclustering and Inverse Cross-Entropy. *Sensors* **21**(19), 6661 (oct 2021). <https://doi.org/10.3390/s21196661>, <http://arxiv.org/abs/2012.01768><https://www.mdpi.com/1424-8220/21/19/6661>
24. Schmarje, L., Grossmann, V., Zelenka, C., Dippel, S., Kiko, R., Oszust, M., Pastell, M., Stracke, J., Valros, A., Volkmann, N., Koch, R.: Is one annotation enough? A data-centric image classification benchmark for noisy and ambiguous label estimation. *arXiv preprint arXiv:2207.06214* (2022), <http://arxiv.org/abs/2207.06214>
25. Schmarje, L., Santarossa, M., Schröder, S.M., Zelenka, C., Kiko, R., Stracke, J., Volkmann, N., Koch, R.: A data-centric approach for improving ambiguous labels with combined semi-supervised classification and clustering. *arXiv preprint arXiv:2106.16209* (2022), <http://arxiv.org/abs/2106.16209>
26. Schousboe, J.T., Rosen, H.R., Vokes, T.J., Cauley, J.A., Cummings, S.R., Nevitt, M.C., Black, D.M., Orwoll, E.S., Kado, D.M., Ensrud, K.E., Others: Prediction models of prevalent radiographic vertebral fractures among older men. *Journal of Clinical Densitometry* **17**(4), 449–457 (2014)
27. Schousboe, J.T., Vo, T., Taylor, B.C., Cawthon, P.M., Schwartz, A.V., Bauer, D.C., Orwoll, E.S., Lane, N.E., Barrett-Connor, E., Ensrud, K.E., Others: Prediction of incident major osteoporotic and hip fractures by trabecular bone score (TBS) and

- prevalent radiographic vertebral fracture in older men. *Journal of Bone and Mineral Research* **31**(3), 690–697 (2016)
28. Schousboe, J.T., Vo, T.N., Langsetmo, L., Taylor, B.C., Kats, A.M., Schwartz, A.V., Bauer, D.C., Cauley, J.A., Ensrud, K.E.: Predictors of change of trabecular bone score (TBS) in older men: results from the Osteoporotic Fractures in Men (MrOS) Study. *Osteoporosis International* **29**(1), 49–59 (2018)
  29. Sohn, K., Berthelot, D., Li, C.L., Zhang, Z., Carlini, N., Cubuk, E.D., Kurakin, A., Zhang, H., Raffel, C.: FixMatch: Simplifying Semi-Supervised Learning with Consistency and Confidence. *Advances in Neural Information Processing Systems 33 pre-proceedings (NeurIPS 2020)* (2020), <http://arxiv.org/abs/2001.07685>
  30. Su, Y., Kwok, T.C.Y., Cummings, S.R., Yip, B.H.K., Cawthon, P.M.: Can classification and regression tree analysis help identify clinically meaningful risk groups for hip fracture prediction in older American men (the MrOS cohort study)? *JBMR plus* **3**(10), e10207 (2019). <https://doi.org/10.1002/jbm4.10207>, <https://onlinelibrary.wiley.com/doi/10.1002/jbm4.10207>
  31. Treece, G.M., Gee, A.H., Tonkin, C., Ewing, S.K., Cawthon, P.M., Black, D.M., Poole, K.E.S., in Men (MrOS) Study, O.F.: Predicting hip fracture type with cortical bone mapping (CBM) in the osteoporotic fractures in men (MrOS) study. *Journal of Bone and Mineral Research* **30**(11), 2067–2077 (2015). <https://doi.org/10.1002/jbmr.2552>
  32. US Preventive Services Task Force, .: Screening for osteoporosis: US preventive services task force recommendation statement. *Annals of internal medicine* **154**(5), 356–364 (2011)
  33. Wang, X., Sanyal, A., Cawthon, P.M., Palermo, L., Jekir, M., Christensen, J., Ensrud, K.E., Cummings, S.R., Orwoll, E., Black, D.M., Others: Prediction of new clinical vertebral fractures in elderly men using finite element analysis of CT scans. *Journal of Bone and Mineral Research* **27**(4), 808–816 (2012)
  34. Watts, N.B.: The fracture risk assessment tool (FRAX®): Applications in clinical practice. *Journal of Women’s Health* **20**(4), 525–531 (2011)
  35. Welch, B.L.: The generalization of ‘student’s’ problem with several different population variances are involved. *Biometrika* **34**(1-2), 28–35 (mar 1947)
  36. Yamamoto, N., Sukegawa, S., Kitamura, A., Goto, R., Noda, T., Nakano, K., Takabatake, K., Kawai, H., Nagatsuka, H., Kawasaki, K., Others: Deep learning for osteoporosis classification using hip radiographs and patient clinical covariates. *Biomolecules* **10**(11), 1534 (2020)
  37. Yang, L., Parimi, N., Orwoll, E.S., Black, D.M., Schousboe, J.T., Eastell, R.: Association of incident hip fracture with the estimated femoral strength by finite element analysis of DXA scans in the Osteoporotic Fractures in Men (MrOS) study. *Osteoporosis International* **29**(3), 643–651 (2018). <https://doi.org/10.1007/s00198-017-4319-2>, <http://link.springer.com/10.1007/s00198-017-4319-2>

## 5 Supplement

Table 4: Overview about individual elements of the risk factor groups

Risk factor group	Individual Elements
Base	age, BMI, height, fat mass, clinic
Multiple	Base + previous fractures spine/hip, osteoporosis in parents, fall history, professional background, previous diseases like cancer or hypertension and smoking and alcohol habits
aBMD	spinal and femoral aBMD
FRAX*	FRAX* 10 year risk for hip and major osteoporotic fracture with and without usage of aBMD
TBS	Average TBS across spine

Table 5: Ablation of hyperparameters on CTN data for 10 and 5 year hip fracture risk – Significant differences to the baseline are marked italic ( $p < 0.05$ ) or bold ( $p < 0.01$ ).

CTN	10 year risk			5 year risk		
	GAP	GAP + Base	GAP + Multiple	GAP	GAP + Base	GAP + Multiple
	80.87 ± 0.13	81.04 ± 0.17	81.66 ± 0.23	88.49 ± 0.32	89.35 ± 0.35	89.62 ± 0.36
Dropout rate 0.4	<i>-0.34</i> (80.53 ± 0.18)	-0.18 (80.87 ± 0.27)	<i>-0.98</i> (80.68 ± 0.33)	-0.47 (88.01 ± 0.37)	-1.14 (88.21 ± 0.43)	<i>-2.00</i> (87.61 ± 0.44)
Min-Max-Normalization	+0.05 (80.92 ± 0.19)	-0.04 (81.00 ± 0.17)	<i>-0.65</i> (81.00 ± 0.25)	-0.15 (88.34 ± 0.43)	-0.99 (88.37 ± 0.37)	-1.21 (88.41 ± 0.54)
Smaller MLP	-0.40 (80.47 ± 0.40)	-0.13 (80.92 ± 0.24)	<i>-0.70</i> (80.95 ± 0.25)	+0.05 (88.54 ± 0.53)	-0.24 (89.12 ± 0.52)	-1.91 (87.70 ± 0.58)
Larger MLP	-0.02 (80.86 ± 0.14)	<b>+0.57</b> (81.61 ± 0.21)	-0.20 (81.46 ± 0.31)	+0.42 (88.91 ± 0.28)	<b>-1.83</b> (87.52 ± 0.25)	<b>-2.32</b> (87.30 ± 0.32)
No input merging	+0.01 (80.88 ± 0.22)	-0.19 (80.86 ± 0.19)	<b>-0.78</b> (80.87 ± 0.19)	+0.72 (89.21 ± 0.41)	<i>-1.60</i> (87.75 ± 0.31)	<b>-3.04</b> (86.58 ± 0.28)
Input merging with s = 1	-0.40 (80.47 ± 0.28)	+0.10 (81.15 ± 0.25)	-0.32 (81.34 ± 0.29)	+0.12 (88.61 ± 0.39)	<i>-1.83</i> (87.52 ± 0.45)	-1.90 (87.72 ± 0.51)

Table 6: Overview of reason for exclusion of patients – We start for all cohorts with the total study population. The reasons for certain exclusions and number of excluded cases are given in white rows and the left over people are given in the grey rows.

	Cohort All			Cohort CT				Cohort X-Ray			
	<i>t</i> = 10 year			<i>t</i> = 10 year		<i>t</i> = 5 year		<i>t</i> = 10 year			
	all	w/o fx	w fx	all	w/o fx	w fx	w/o fx	w fx	all	w/o fx	w fx
Start	5994	5994	5994	5994	5994	5994	5994	5994	5994	5994	5994
Not all risk factors present	N/A	N/A	N/A	52	52	52	52	52	52	52	52
	5994	5994	5994	5942	5942	5942	5942	5942	5942	5942	5942
No Image Data	N/A	N/A	N/A	2670	2670	2670	2670	2670	1759	1759	1759
	5994	5994	5994	3272	3272	3272	3272	3272	4183	4183	4183
Censored	N/A	1805	1805	N/A	970	970	970	970	N/A	762	762
	5994	4189	4189	3272	2302	2302	2302	2302	4183	3421	3421
Both Hips not usable	N/A	N/A	N/A	107	72	72	72	72	288	224	224
	5994	4189	4189	3165	2230	2230	2230	2230	3895	3197	3197
Wrong Class	N/A	185	4004	N/A	80	2150	32	2198	N/A	89	3108
<i>n</i>	5994	4004	185	3165	2150	80	2198	32	3895	3108	89